Materials and Design 195 (2020) 108993

Contents lists available at ScienceDirect

Materials and Design

journal homepage: www.elsevier.com/locate/matdes

Thickness gradient promotes the performance of Si-based anode material for lithium-ion battery

Zhenbin Guo [a,b], Haimin Yao [a,b,*]

[a] The Hong Kong Polytechnic University Shenzhen Research Institute, Shenzhen 515057, China
[b] Department of Mechanical Engineering, The Hong Kong Polytechnic University, Hung Hom, Kowloon, China

HIGHLIGHTS

- Thickness gradient enables a Si-based electrode to uphold specific capacity above 1000 mAh g^{-1} for more than 100 cycles.
- Thickness gradient promotes the energy density of a Si-based electrodes after 100 cycles by more than 16 times.
- The gradient-thickness strategy significantly enhances the performance of LIB electrode at zero additional cost in materials.

GRAPHICAL ABSTRACT

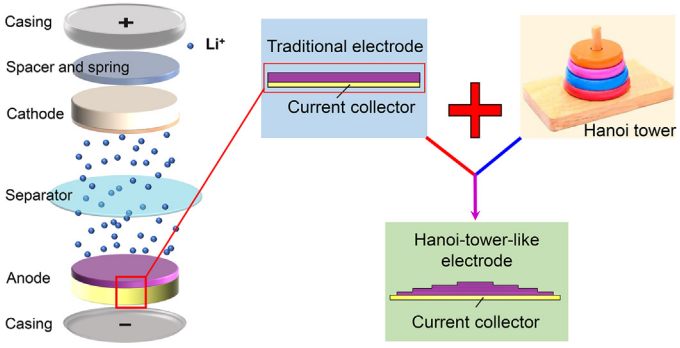

ARTICLE INFO

Article history:
Received 20 June 2020
Received in revised form 24 July 2020
Accepted 24 July 2020
Available online 28 July 2020

Keywords:
Lithium-ion battery
Electrode material
Thin film
Interface
Delamination

ABSTRACT

The large volume change of the silicon (Si) during the lithiation and delithiation process has long been a problem impeding its application as one of the most promising anode materials for lithium-ion batteries (LIBs). In this paper, we proposed a conceptually new idea to address this problem simply by tapering the thickness of the electrode material film. The resulting thickness-gradient electrode exhibits considerable enhancement in the electrochemical performances including capacity, capacity retention, energy density, Coulombic efficiency, and rate capability in comparison to the traditional counterparts with uniform thickness. Such enhancement in the electrochemical performance can be attributed to the lessening of the stress concentration on the interface between the electrode film and the current collector upon the volume change of Si taking place in the lithiation and delithiation process. To make the best use of this strategy, the optimal design of the gradient thickness is proposed based on the theory of stress homogenization, followed by the experimental verification. The results of this paper provide a facile, cost-effective, and scalable way for enhancing the performance of Si-based anodes for LIBs. This strategy can be further extended to the other anode materials suffering the similar lithiation-induced volume change problem.

1. Introduction

Among diverse devices for energy storage, lithium-ion battery (LIB) stands out for its comparatively high capacity, better rate capability, and longer lifespan [1]. Nevertheless, recently with the ever-increasing demand for high-performance power supply in industries and personal electronics, the limitation of the capacity of the prevalent carbon-based LIBs starts to emerge [2]. Developing next-generation LIB with higher capacity and cyclability is believed to provide a mighty thrust to the development of technology and the global economy. A straightforward measure to improve the capacity of LIB is to replace the carbon with other electrode materials with a higher capacity [3–5]. However, a

* Corresponding author at: The Hong Kong Polytechnic University Shenzhen Research Institute, Shenzhen 515057, China.
E-mail address: mmhyao@polyu.edu.hk (H. Yao).

https://doi.org/10.1016/j.matdes.2020.108993

common problem existing in the anode materials with high capacity is the large volume change (LVC) during the lithiation and delithiation process, which will cause the pulverization of the electrode material film as well as detachment from the current collector [6–8]. As one of the most representative examples, Silicon (Si) possesses theoretical specific capacity as high as 4200 mAh g^{-1}, which is one order of magnitude higher than that of the graphite [9,10]. However, the lifespan of the Si-based LIBs is much shorter than that of the carbon-based counterparts. This can be attributed to the LVC (300–400%) of the Si during the lithiation and delithiation processes [11,12]. To tackle the LVC problem of Si, a bunch of research efforts has been made [13–24], including the application of constraining coating on Si materials [25–27], structurization of the Si nanomaterials such as 0-dimensional nanoparticles [28,29], 1-dimensional nanowires [30–32] and 2-dimensional thin films [33,34]. Despite the success of these approaches in alleviating the LVC problem of Si [35–38], the sophisticated chemical processes and expensive fabrication facilities involved greatly limit the transfer of these techniques to the existing LIB industry. To find a facile, cost-effective, and scalable solution to the LVC problem of Si, we cast our attention to the interface between the electrode film and current collector.

From a mechanical point of view, the interface between the electrode film and the underlying current collector is the Achilles heel of this bilayer structure, because the strain misfit across the interface, which may be induced by the volume change of the electrode film during lithiation and delithiation, will lead to significant stress and strain concentration and singularity [39–42]. Interfacial delamination tends to occur after sufficient cycles of charging and discharging, resulting in the degradation of the electrochemical performance. Suppressing the interfacial stress and strain concentration is thus believed beneficial for solving of the LVC problem of Si. Inspired by the success of functionally graded material (FGM) in alleviating the interfacial stress concentration [43–45], we have purposely altered the concentration of Si nanoparticles in the thickness direction of the electrode film. The resulting graded electrode exhibits elevated electrochemical performance in comparison to the traditional ones [46]. The gain of such performance enhancement involves no additional materials and chemical processes. This success implies the great promise of gradient thickness as another strategy for homogenizing interfacial stress discovered recently [47].

To testify the feasibility of the gradient thickness in addressing the LVC problem of Si-based anode, in this paper we deliberately change the thickness of a circular Si-based anode film, which is traditionally uniform, to be tapering along the radial direction, as shown schematically in Fig. 1a. In view of the practical difficulty in fabricating such continuously variable thickness, an approximate substitute is proposed by stacking multiple thinner sublayers with different and descending diameters, resulting in an electrode with stepwise gradient thickness (Fig. 1b). The remainder of this paper is structured as follows. Firstly, the detailed manufacturing process and electrochemical characterization are introduced. Then, the obtained results are discussed to show the effectiveness of the thickness gradient in promoting the electrochemical performance of LIBs. To make the best use of this strategy, the optimal design of the gradient thickness is explored in both theory and experiment. Finally, the paper is concluded by comparing the current strategy with the similarities that were proposed earlier. Our results in this paper provide a novel and practical strategy for enhancing the electrochemical performances of Si-based electrodes at zero additional cost in materials, which is believed to have a great promise of application in the design of next-generation LIBs.

2. Experimental procedure

2.1. Preparation of Si-based uniform electrodes for LIB through spray painting

Traditionally, the electrode material of LIB is cast onto the current collector (Cu foil) by using a film applicator. The thickness of the resulting film of the electrode material is normally uniform. To prepare electrode film with gradient thickness, spray painting technique is applied with an apertured disk used as the mask. The process is elaborated as follows.

Firstly, the Si-based electrode material is prepared by mixing Si NPs, carbon black (conductive agent), and PVDF (binder) with solvent N-Methyl-2-pyrrolidone (NMP) in a mass ratio of 3:1:1:30 using pestle and mortar. Then, the as-prepared slurry is filled into the container of the spray gun and spraying is carried out towards the copper (Cu) foil with an apertured mask applied amid to control the size of the region that can receive the spray on the Cu foil (Fig. 2a). The thickness of the electrode film is controlled by tuning the spraying time, while other affecting parameters such as the slurry concentration, air pressure, and distance between the spray gun and Cu foil, are kept fixed. After the spraying, the Cu foil together with the deposited electrode film and the mask is dried at 80 °C for 3 h followed by 10 h at 120 °C in a vacuum oven. The area of the dried electrode film on the Cu foil exhibits similar size to that of the aperture on the mask (Fig. 2b). After removing the mask and punchcutting the electrode film together with the underlying Cu foil (Fig. 2c), a disk-like Si-based electrode for LIB is obtained. The subsequent measurement indicates that the thickness of the prepared electrode film (dried) grows with the spraying time in a nonlinear manner (Fig. 3a). Initially, the growth rate is 0.65 μm/s. As the spraying proceeds, the growth rate decreases and finally saturates at 0.05 μm/s.

2.2. Preparation of Hanoi-tower-like electrodes through multiple spraying

The method of spraying developed above allows us to prepare electrode film with gradient thickness by multiple steps of spraying in combination with the application of masks with descending aperture sizes. The resulting electrode film exhibits thickness with a stepwise gradient depending on the aperture size and the number of the masks applied and the spraying time in each step (Fig. 4a). Due to the resemblance to the Hanoi-tower in morphology, the electrode with such stepwise thickness is called Hanoi-tower-like (HTL) electrode hereafter. Fig. 4b shows the evolution of the electrode film (dried) after 1, 2, and 3 steps of spraying. To prepare the HTL electrodes in a controllable way, the thickness growth in each spraying step should be characterized quantitively in advance. Surprisingly, if the spraying is conducted on a pre-deposited and dried electrode film rather than on a Cu foil, the thickness of the electrode film will grow linearly with the spraying time at a growth rate of 0.15 μm/s (Fig. 3b). This is different from the growth rate of the electrode film directly deposited on the Cu foil, which might be attributed to the re-wetting and deformation of the pre-deposited film caused by the subsequent spraying.

2.3. Electrochemical characterization

The electrochemical performance of the as-prepared electrode is characterized using CR2032 coin-type half-cells with Lithium foil (Shenzhen Teensky Technology Co. Ltd) being employed as the counter electrode, polypropylene Celgard 2400 as the separator (Celgard), 1 M LiPF6 in ethylene carbonate and diethyl carbonate (EC:DEC = 1:1) with a 5 vol% fluoroethylene carbonate (FEC) and 1 vol% vinylene carbonate (VC) additive as the electrolyte (DoDoChem Co. Ltd). Galvanostatic discharge/charge test is carried out with a battery tester (LAND CT-2001A) at the potential ranging from 0.01 to 1.2 V vs. Li^+/Li. All electrochemical cycling measurements are carried out at room temperature. All the specific capacities and current density are assessed based on the weight of Si applied.

3. Results and discussion

Three-layer (3 L) and seven-layer (7 L) HTL electrodes were prepared and characterized by using the multiple spraying method introduced above (see Table S1 and Table S2 for the detailed fabrication

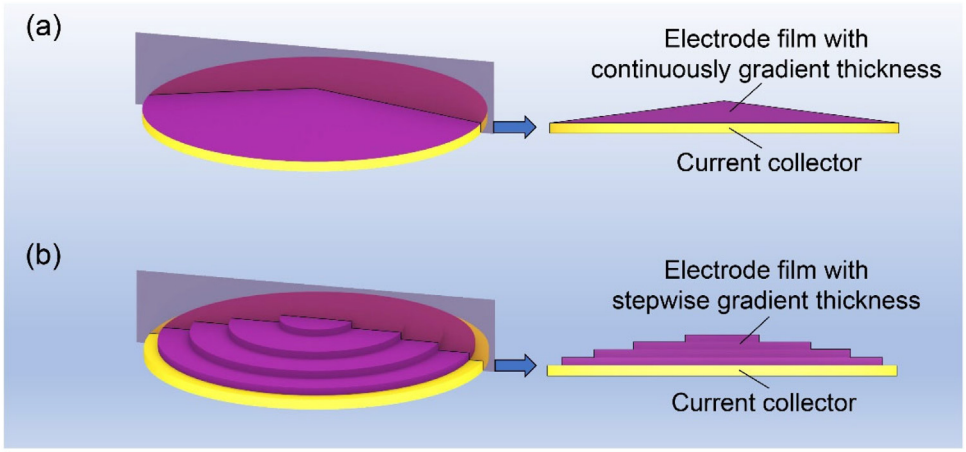

Fig. 1. Schematics of electrodes with (a) continuously gradient thickness, and (b) stepwise gradient thickness.

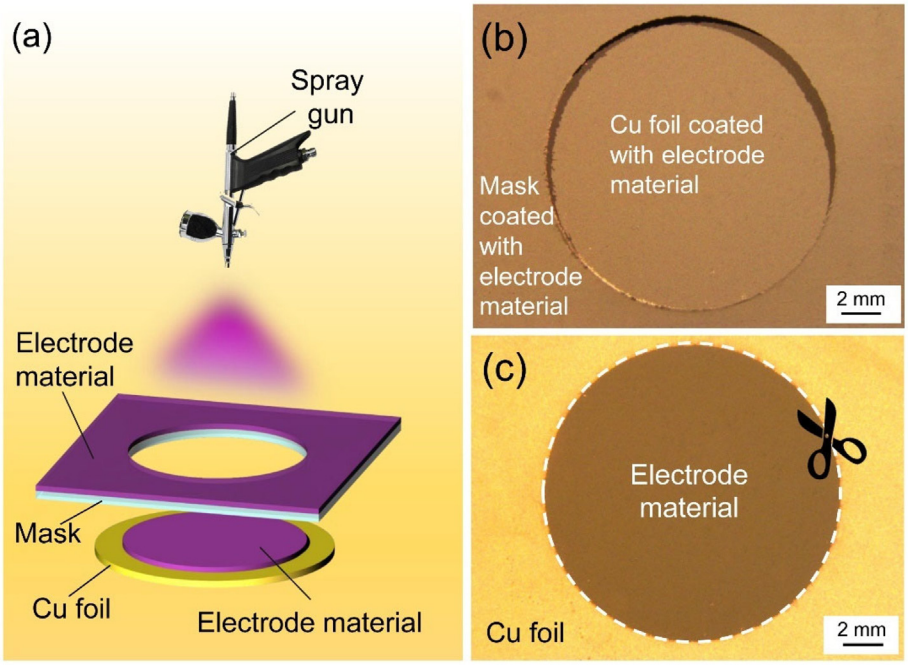

Fig. 2. (a) Schematic illustration of the spraying-based method for fabricating electrodes for LIB; (b) Optical microscope image (top view) of a masked Cu foil after spraying and drying; (c) Optical microscope image (top view) of a Cu foil deposited with a circular film of Si-based electrode material.

parameters). For comparison, electrodes with the same constituents and mass loading but uniform thickness were prepared, including the uniform electrodes prepared by casting and spraying methods, respectively. The average specific charge capacity of the half-cells of each type of electrodes is shown in Fig. 5a, b. Comparing two types of uniform electrodes prepared by different methods, the electrochemical performance shows a certain dependence on the manufacturing method. In particular, an electrode prepared by casting performs better than that prepared by spraying especially in the initial 20 cycles. The average specific charge capacity ($N = 5$) of the uniform electrodes by casting is 568 mAh g^{-1} after 10 cycles and will dry out after 30 cycles, while the average specific charge capacity ($N = 5$) of the uniform electrode prepared by spraying is 198 mAh g^{-1} after 10 cycles and will dry out after 20 cycles. In comparison to the electrodes with uniform thickness, the 3 L-HTL electrode exhibits a much higher specific capacity. The average specific charge capacity ($N = 3$) of the 3 L-HTL electrodes is 1408 mAh g^{-1} after 10 cycles, 906 mAh g^{-1} after 50 cycles, and 684 mAh g^{-1} after 100 cycles, respectively. The benefit of gradient thickness can be further extracted if we increase the layer number from 3 to 7. In particular, the average specific charge capacity ($N = 3$) of the 7 L-HTL electrodes is 2574 mAh g^{-1} at the first cycle and 976 mAh g^{-1} after 100 cycles.

Fig. 5c shows the galvanostatic discharge/charge profiles of the 7 L-HTL electrode at the voltage range of 0.01–1.20 V and a rate of 210 mA g^{-1} at selected cycles. When Li-ions get inserted into the electrode with gradient thickness for the first time (discharging or lithiation process), the voltage drops drastically to 0.14 V, followed by a steady plateau and then a progressive decrease to 0.01 V. During the ensuing charging (delithiation) process, the voltage initially increases quickly, followed by a relatively steady plateau ranging from 0.22 V to 0.48 V. Similar plateaus can be observed even after 100 cycles, implying a stable voltage window for charging and discharging. In contrast, for the uniform electrode prepared by casting, the voltage plateau is only observed in the first few cycles and disappears after the 10^{th} cycle (Fig. 5d).

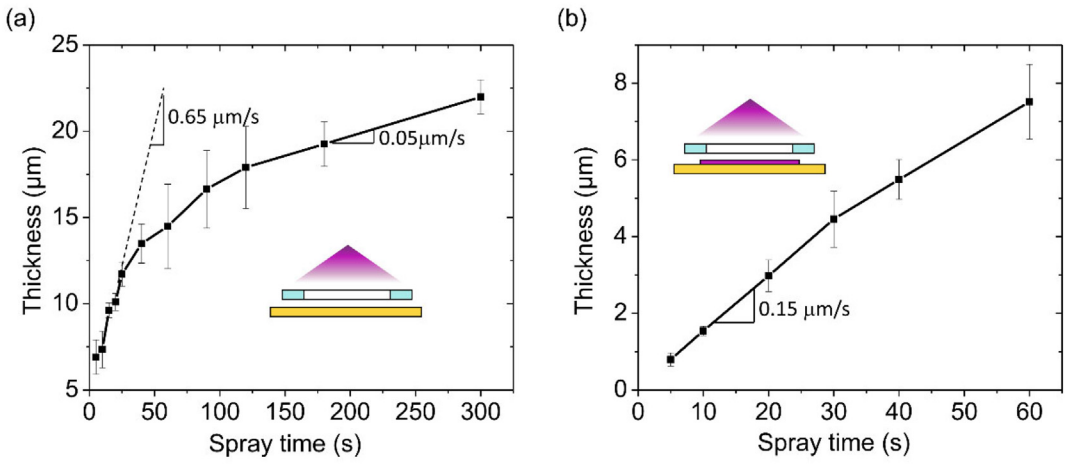

Fig. 3. Variation of the thickness of the deposited film with the spraying time for (a) spraying directly on Cu foil, and (b) spraying on a pre-deposited and dried electrode film.

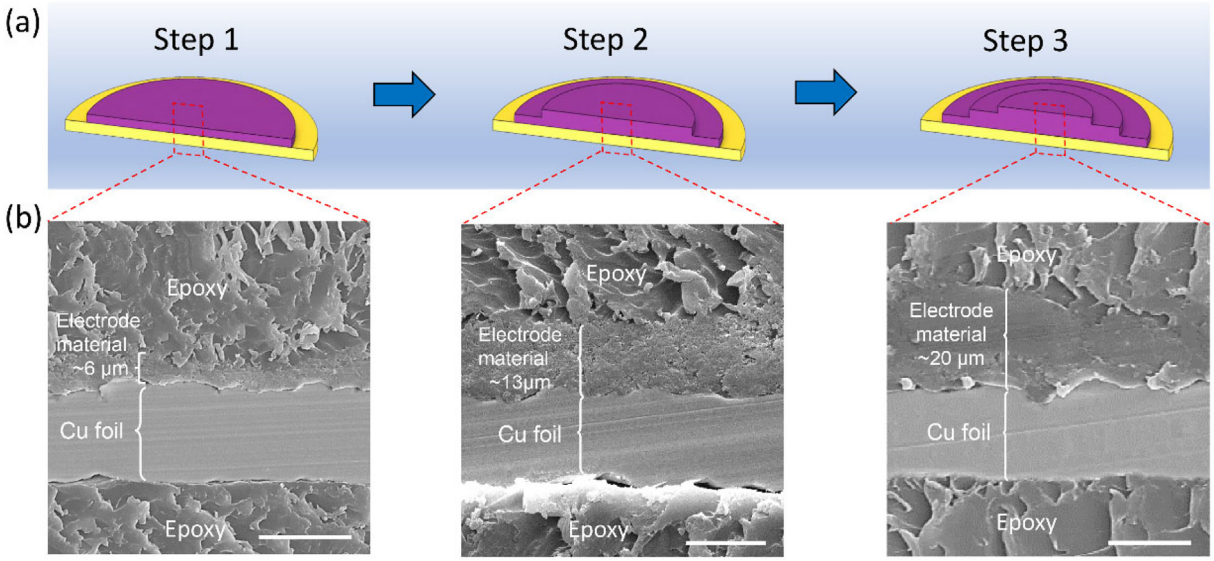

Fig. 4. Cross-sectional SEM images of the electrode showing the thickness of electrode film after each step of spraying. Scale bar: 15 μm.

The galvanostatic profiles shown in Fig. 5c and d allows us to compare the gravimetric energy density (U_m) of these two types of electrodes, which can be calculated through $U_m = \varphi_{Si} \int V d\ (C_{Si})$, where φ_{Si} is the mass fraction of the Si in the electrode material (i.e., 60%), V is the potential vs. Li/Li^+, and C_{Si} is the specific capacity of Si. This integration actually equals the area underneath the galvanostatic charge profiles as illustrated by the green shaded areas in Fig. 5c, d. The calculated gravimetric energy densities for the electrodes with gradient thickness and uniform thickness at the selected cycles are shown in Table S3. It can be seen that the gradient electrode exhibits higher gravimetric energy density as compared to the uniform counterpart, especially at a higher cycle number. For example, at the 100^{th} cycle, the gravimetric energy density of the gradient electrode is more than 16 times that of the uniform one. This conclusion also applies to the volumetric energy density because in our study, all the electrode materials are prepared following the same ingredient formula and the amount of electrode materials loaded on the current collectors is maintained the same no matter the thickness of the electrode film is uniform or gradient.

Fig. 5e compares the Coulombic efficiency of these two types of electrodes. It can be seen that the initial Coulombic efficiency of the 7 L-HTL electrode is around 74% (with initial discharge and charge capacities being 3225 and 2377 mAh g^{-1}, respectively) which is higher than 63%, the initial Coulombic efficiency of the uniform electrode prepared by casting whose initial discharge and charge capacities are 3234 and 2052 mAh g^{-1}, respectively. This implies that the electrode film with gradient thickness can effectively enhance the utilization efficiency of Si in the electrode.

The rate capability of the 7 L-HTL electrode, which reflects the degradation of performance of the LIB at a higher charge/discharge rate, is compared with that of the conventional uniform electrode in Fig. 5f. At the same discharge/charge rate varying from 0.05C to 1C (1C = 4200 mA g^{-1}), the 7 L-HTL electrode always delivers a higher specific capacity than the uniform one does. When the rate returns to 0.05C, the specific capacity of the 7 L-HTL electrode is 1184 mAh g^{-1}, which greatly overpasses that of the uniform one (208 mAh g^{-1}). These results indicate that the electrode film with gradient thickness can significantly improve the rate capability of Si-based LIB.

The success of the HTL electrode in enhancing the cycling performance of LIB motivates us to explore the optimal design of the gradient thickness that can bring us the maximum profit of this strategy. Since the mechanism accounting for such success is the lessening of the stress concentration and singularity by the gradient thickness, maximum profit is expected if one can achieve a completely uniform shear stress

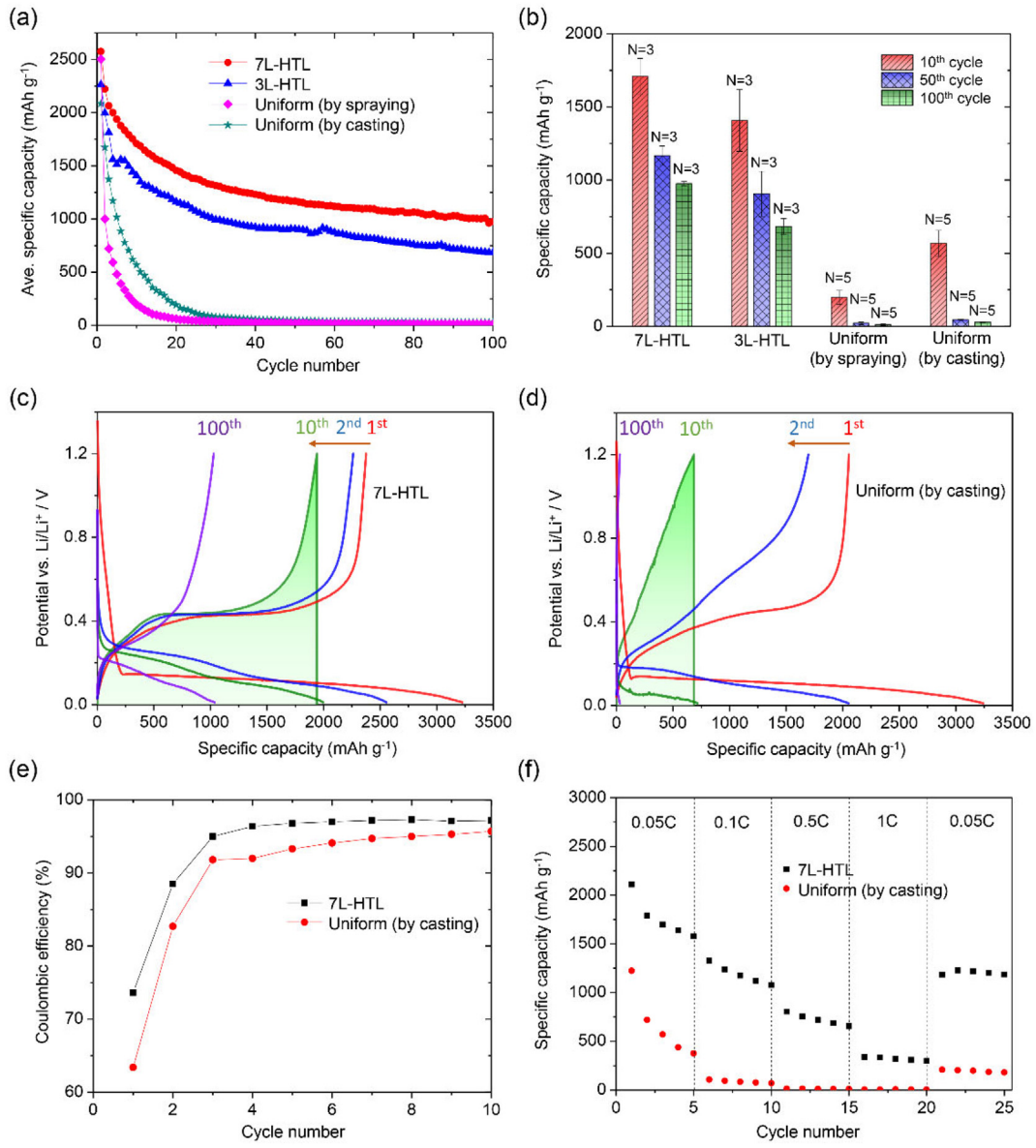

Fig. 5. (a) The average specific charge capacity of the 7 L-HTL electrodes ($N = 3$), 3 L-HTL electrodes ($N = 3$), uniform electrodes prepared by spraying ($N = 5$) and uniform electrodes prepared by casting ($N = 5$) during cycling test at the voltage between 0.01 V and 1.2 V vs. Li/Li^+ and a rate of 0.05C; (b) Comparison of the specific capacity at the selected cycles. Here, N is the number of tested half-cells; The 1st, 2nd, 10th, and 100th galvanostatic discharge/charge profiles of (c) a 7 L-HTL electrode and (d) a uniform electrode prepared by casting. Here the green shaded areas represent the gravimetric energy densities (U_m) of both electrodes at the 10th cycle. (e) Coulombic efficiency of a 7 L-HTL electrode in comparison to that of a uniform electrode prepared by casting. (f) The rate capability of a 7 L-HTL electrode in comparison to that of a uniform electrode prepared by casting at a rate varying from 0.05C to 1C. (For interpretation of the references to colour in this figure legend, the reader is referred to the web version of this article).

field on the interface when strain misfit is present. This question actually has been systematically discussed in our previous work for different configurations of bi-material systems [47]. Specifically, for a circular electrode film, the optimal thickness profile of the film is analytically given by

$$t_e(r) = \frac{(1-\nu_e^2)E_c t_c}{(1-\nu_c^2)E_e}\left\{\left[\frac{(\nu_e+2)(1-\nu_c^2)+\left[\frac{3E_c t_c \varepsilon_{mis}}{R\tau_{exp}}-(\nu_c+2)(1-\nu_c)\right](\nu_e+1)}{(\nu_e+2)(1-\nu_c^2)\cdot\frac{r}{R}+\left[\frac{3E_c t_c \varepsilon_{mis}}{R\tau_{exp}}-(\nu_c+2)(1-\nu_c)\right](\nu_e+1)}\right]^{\frac{3}{2+\nu_e}}-1\right\} \quad (1)$$

where r is the distance from the film center; E_e and ν_e are Young's modulus and Poisson's ratio of the electrode film, respectively; E_c and ν_c are Young's modulus and Poisson's ratio of the current collector, respectively; t_c and R are the thickness and radius of the current collector, respectively; ε_{mis} is the strain misfit between the electrode film and current collector (Cu foil) caused by the intrinsic volume change of Si during the process of lithiation and delithiation; τ_{exp} is the expected homogeneous interfacial shear stress at strain misfit of ε_{mis}. In physics, τ_{exp} is capped by the shear strength of the interface. For given E_e, ν_e, E_c, ν_c, t_c, and R, Eq. (1) indicates that the gradient thickness $t_e(r)$ is correlated to the ratio of $\tau_{exp}/\varepsilon_{mis}$, which represents the growth rate of the expected homogeneous shear stress on the interface with the increase of strain misfit, and therefore can be deemed as the shearing stiffness of the interface corresponding to that gradient thickness.

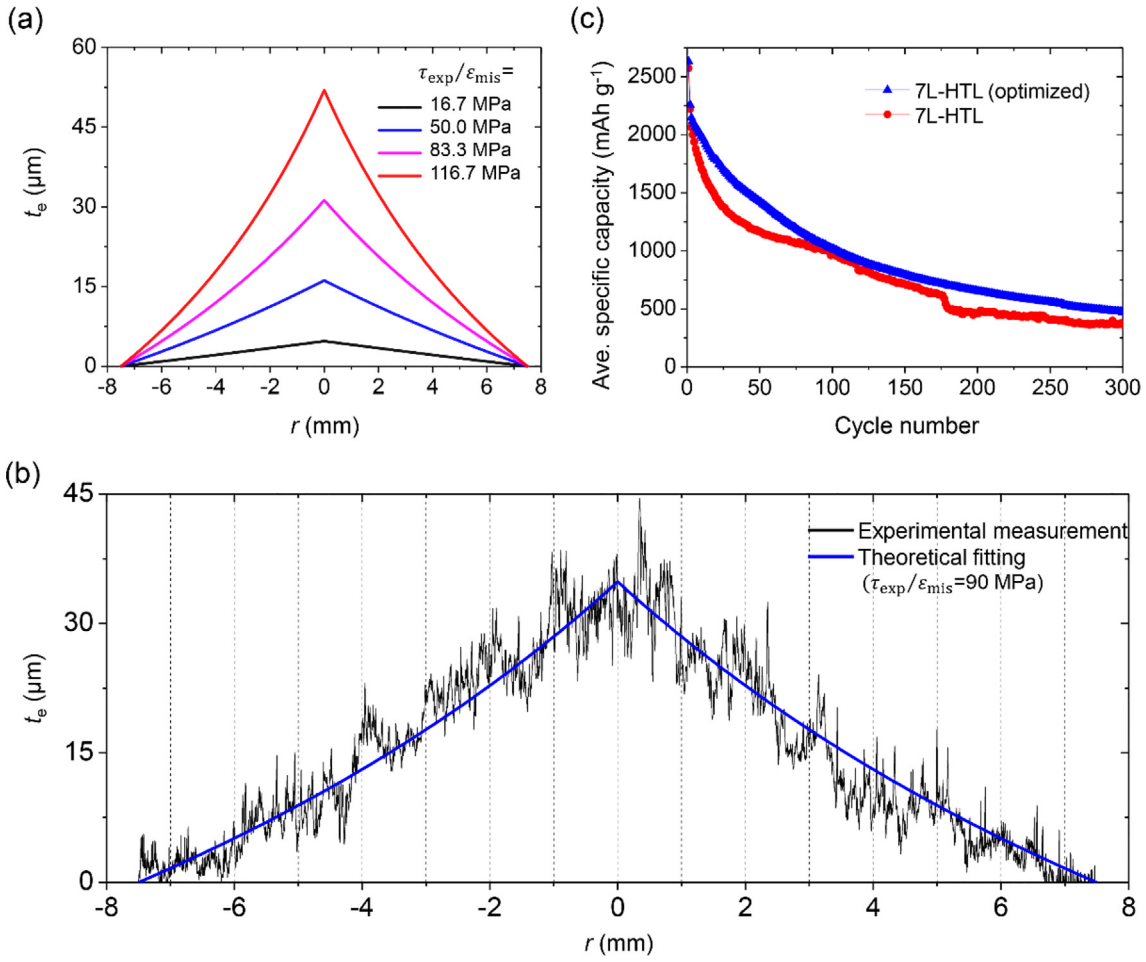

Fig. 6. (a) The optimal profiles of electrode films corresponding to different shearing stiffnesses of the interface ($\tau_{exp}/\varepsilon_{mis}$). Here, the base diameter of the circular electrode is taken as 15 mm. (b) The measured topography of an optimized 7 L-HTL electrode. (c) The average specific charge capacity ($N = 3$) of the optimized 7 L-HTL electrodes in comparison to that of the unoptimized ones.

Taking $E_e = 19.7$ GPa [48], $\nu_e = 0.3$ (assumed), $E_c = 128$ GPa, $\nu_c = 0.33$ [49], $t_c = 10$ μm, $R = 7.5$ mm in Eq. (1), the cross-sectional profile of the optimal thickness $t_e(r)$ is plotted in Fig. 6a for different shearing stiffnesses of $\tau_{exp}/\varepsilon_{mis}$. It can be seen that the cross-sectional profile of the optimal thickness exhibits a tent-like shape. The higher the tent, the greater the resulting interfacial shearing stiffness $\tau_{exp}/\varepsilon_{mis}$.

Following the guideline by the theoretical solution to the optimal profile of the gradient thickness, we prepared an optimized 7 L-HTL (see Table S4 for the detailed fabrication parameters). Topographical characterization with a surface profiler (Dektak XT) along the radial direction indicates that the manufactured profile is quite close to the theoretical solution to the optimal profile corresponding to $\tau_{exp}/\varepsilon_{mis} =$ 90 MPa (Fig. 6b). Subsequent electrochemical characterization on the

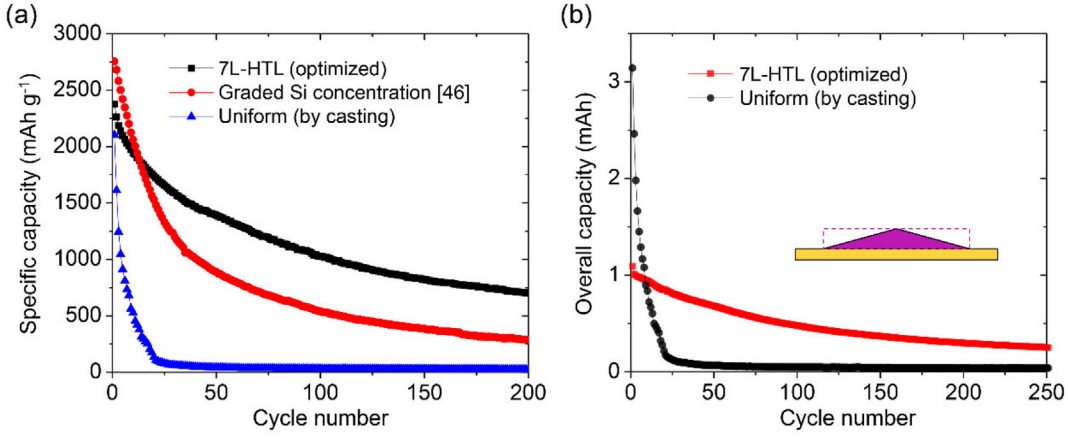

Fig. 7. (a) Comparison of the cycling performance of an electrode with gradient thickness (optimized 7 L-HTL) and an electrode with gradient in Si composition developed in our previous study [46]; (b) Comparison of the cycling performance of a 7 L-HTL electrode with a uniform electrode (as depicted by the broken line in the inset) with the same height (~15 μm).

optimized 7 L-HTL electrode exhibits a better cycling performance compared to that of the unoptimized ones (Fig. 6c). In particular, the average specific charge capacity ($N = 3$) of the optimized 7 L-HTL electrodes is 2633 mAh g^{-1} at the first cycle, 1990 mAh g^{-1} after 10 cycles, 1019 mAh g^{-1} after 100 cycles and 472 mAh g^{-1} after 300 cycles, respectively. Such enhancement in the electrochemical performance also outruns the enhancement brought by the gradient in Si concentration as discovered in our previous study [46] (Fig. 7a).

For a practical battery cell, what is more important is its overall capacity, which reflects the total amount of energy that can be stored, rather than the specific capacity of the active material. This is because the specific capacity of the active material (e.g., Si) tends to decrease as the mass loading increases. The preceding discussion has demonstrated the advantage of gradient thickness over the uniform thickness in the aspect of specific capacity. It is practically worthy of making a comparison between the gradient and uniform electrodes from the perspective of overall capacity. For this purpose, we compare the overall capacities of an optimized 7 L-HTL electrode (see Table S5 for the detailed fabrication parameters) and a uniform control with the same film height (Fig. 7b). It can be seen that the overall capacity of the uniform electrode drops quickly with the increasing cycle number. After about 9 cycles, the overall capacity of the uniform electrode drops below that of the 7 L-HTL electrode even though more active material (Si) is contained in the uniform electrode than in the gradient one. Therefore, the gradient electrode achieves a higher overall capacity with the use of less active material. This feature implies the great promise and value of the gradient-thickness electrode for the cost control in the LIB industry.

4. Conclusion

In this paper, we tackled the LVC problem of the Si-based electrodes simply by introducing the thickness gradient into the electrode film. The resulting gradient electrodes with descending thickness exhibit much better cycling performance in comparison to the traditional uniform ones as well as the ones with graded Si concentration. The optimal design of the gradient thickness is discovered, allowing us to make the best use of the strategy of gradient thickness. In comparison to the other strategies for addressing the LVC problem of Si, this strategy is facile to implement and cost-effective and involves no additional chemical processes and materials. The scaling up of this method in the existing battery industry is relatively easy. Admittedly, the electrode films that we fabricated above with the spraying-based method achieved only a stepwise gradient in thickness. For electrode films with continuous gradient, which may bring additional enhancement to the electrochemical performance, sophisticated technique such as additive manufacturing should be adopted.

Although our discussion on the gradient-thickness electrodes has been made based on the circular electrode, this concept can be extended to the rectangular electrode. However, due to the geometry complexity, it is scarcely possible to obtain the analytical solution to the optimal thickness gradient for the rectangular ones. A numerical approach should be applied to determine the form of the gradient thickness, whereby the interfacial shearing stress is homogenized as has been systematically discussed in our previous work [47]. Detailed discussion on the rectangular electrode exceeds the scope of the present paper and is left to the future work. Our results in this paper provide a conceptually new idea for addressing the LVC problem of Si and is believed to promote the application of anode materials with large specific capacity like Si in the next-generation LIBs.

Author contribution

H.Y. conceived the idea and supervised the project; Z.G. conducted the fabrication, characterization and data analysis; Z.G. and H.Y. prepared the manuscript together.

Declaration of Competing Interest

On the behalf of all authors, I wish to confirm that there are no known conflicts of interest associated with this publication and there has been no significant financial support for this work that could have influenced its outcome.

We confirm that the manuscript has been read and approved by all named authors and that there are no other persons who satisfied the criteria for authorship but are not listed. We further confirm that the order of authors listed in the manuscript has been approved by all of us.

We confirm that we have given due consideration to the protection of intellectual property associated with this work and that there are no impediments to publication, including the timing of publication, with respect to intellectual property. In so doing we confirm that we have followed the regulations of our institutions concerning intellectual property.

We understand that the Corresponding Author is the sole contact for the Editorial process (including with the other authors about progress, submissions of revisions and final approval of proofs). We confirm that we have provided a current, correct email address which is accessible by the Corresponding Author and which has been configured to accept email from mmhyao@polyu.edu.hk.

Acknowledgements

This work was supported by the National Natural Science Foundation of China (11772283).

Appendix A. Supplementary data

Supplementary data to this article can be found online at https://doi.org/10.1016/j.matdes.2020.108993.

References

[1] M. Armand, J.M. Tarascon, Building better batteries, Nature 451 (7179) (2008) 652–657.
[2] J.M. Tarascon, M. Armand, Issues and challenges facing rechargeable lithium batteries, Nature 414 (6861) (2001) 359–367.
[3] B. Kang, G. Ceder, Battery materials for ultrafast charging and discharging, Nature 458 (7235) (2009) 190–193.
[4] M.K. Chan, C. Wolverton, J.P. Greeley, First principles simulations of the electrochemical lithiation and delithiation of faceted crystalline silicon, J. Am. Chem. Soc. 134 (35) (2012) 14362–14374.
[5] M.R. Palacin, Recent advances in rechargeable battery materials: a chemist's perspective, Chem. Soc. Rev. 38 (9) (2009) 2565–2575.
[6] X.H. Liu, L. Zhong, S. Huang, S.X. Mao, T. Zhu, J.Y. Huang, Size-dependent fracture of silicon nanoparticles during lithiation, ACS Nano 6 (2) (2012) 1522–1531.
[7] S. Huang, F. Fan, J. Li, S. Zhang, T. Zhu, Stress generation during lithiation of high-capacity electrode particles in lithium ion batteries, Acta Mater. 61 (12) (2013) 4354–4364.
[8] M.J. Chon, V.A. Sethuraman, A. McCormick, V. Srinivasan, P.R. Guduru, Real-time measurement of stress and damage evolution during initial lithiation of crystalline silicon, Phys. Rev. Lett. 107 (4) (2011), 045503. .
[9] Y.P. Wu, E. Rahm, R. Holze, Carbon anode materials for lithium ion batteries, J. Power Sources 114 (2) (2003) 228–236.
[10] M. Endo, C. Kim, K. Nishimura, T. Fujino, K. Miyashita, Recent development of carbon materials for Li ion batteries, Carbon 38 (2) (2000) 183–197.
[11] N. Spinner, L. Zhang, W.E. Mustain, Investigation of metal oxide anode degradation in lithium-ion batteries via identical-location TEM, J. Mater. Chem. A 2 (6) (2014) 1627–1630.
[12] B.A. Boukamp, G.C. Lesh, R.A. Huggins, All-solid lithium electrodes with mixed-conductor matrix, J. Electrochem. Soc. 128 (4) (1981) 725–729.
[13] X. Xiao, P. Liu, M.W. Verbrugge, H. Haftbaradaran, H. Gao, Improved cycling stability of silicon thin film electrodes through patterning for high energy density lithium batteries, J. Power Sources 196 (3) (2011) 1409–1416.
[14] H. Haftbaradaran, X. Xiao, M.W. Verbrugge, H. Gao, Method to deduce the critical size for interfacial delamination of patterned electrode structures and application to lithiation of thin-film silicon islands, J. Power Sources 206 (2012) 357–366.
[15] Y. Yao, K. Huo, L. Hu, N. Liu, J.J. Cha, M.T. McDowell, P.K. Chu, Y. Cui, Highly conductive, mechanically robust, and electrochemically inactive TiC/C nanofiber scaffold for high-performance silicon anode batteries, ACS Nano 5 (10) (2011) 8346–8351.

[16] B. Koo, H. Kim, Y. Cho, K.T. Lee, N.S. Choi, J. Cho, A highly cross-linked polymeric binder for high-performance silicon negative electrodes in lithium ion batteries, Angew. Chem. Int. Ed. 51 (35) (2012) 8762–8767.
[17] M. Zheng, C. Wang, Y. Xu, K. Li, D. Liu, A water-soluble binary conductive binder for Si anode lithium ion battery, Electrochim. Acta 305 (2019) 555–562.
[18] D. Mazouzi, D. Reyter, M. Gauthier, P. Moreau, D. Guyomard, L. Roué, B. Lestriez, Very high surface capacity observed using Si negative electrodes embedded in copper foam as 3D current collectors, Adv. Energy Mater. 4 (8) (2014) 1301718.
[19] Y.L. Kim, Y.K. Sun, S.M. Lee, Enhanced electrochemical performance of silicon-based anode material by using current collector with modified surface morphology, Electrochim. Acta 53 (13) (2008) 4500–4504.
[20] L. Chen, K. Wang, X. Xie, J. Xie, Effect of vinylene carbonate (VC) as electrolyte additive on electrochemical performance of Si film anode for lithium ion batteries, J. Power Sources 174 (2) (2007) 538–543.
[21] L. Chen, K. Wang, X. Xie, J. Xie, Enhancing electrochemical performance of silicon film anode by vinylene carbonate electrolyte additive, Electrochem. Solid-State Lett. 9 (11) (2006) 512–515.
[22] R. Yi, F. Dai, M.L. Gordin, S. Chen, D. Wang, Micro-sized Si-C composite with interconnected nanoscale building blocks as high-performance anodes for practical application in lithium-ion batteries, Adv. Energy Mater. 3 (3) (2013) 295–300.
[23] I. Kang, J. Jang, M.S. Kim, J.W. Park, J.H. Kim, Y.W. Cho, Nanostructured silicon/silicide/carbon composite anodes with controllable voids for Li-ion batteries, Mater. Des. 120 (2017) 230–237.
[24] L. Yue, L. Zhang, H. Zhong, Carboxymethyl chitosan: a new water soluble binder for Si anode of Li-ion batteries, J. Power Sources 247 (2014) 327–331.
[25] C.M. Wang, X. Li, Z. Wang, W. Xu, J. Liu, F. Gao, L. Kovarik, J.G. Zhang, J. Howe, D.J. Burton, Z. Liu, X. Xiao, S. Thevuthasan, D.R. Baer, In situ TEM investigation of congruent phase transition and structural evolution of nanostructured silicon/carbon anode for lithium ion batteries, Nano Lett. 12 (3) (2012) 1624–1632.
[26] S.H. Ng, J. Wang, D. Wexler, K. Konstantinov, Z.P. Guo, H.K. Liu, Highly reversible lithium storage in spheroidal carbon-coated silicon nanocomposites as anodes for lithium-ion batteries, Angew. Chem. Int. Ed. 45 (41) (2006) 6896–6899.
[27] M.E. Stournara, Y. Qi, V.B. Shenoy, From ab initio calculations to multiscale design of Si/C core-shell particles for Li-ion anodes, Nano Lett. 14 (4) (2014) 2140–2149.
[28] A. Wilson, J. Dahn, Lithium insertion in carbons containing nanodispersed silicon, J. Electrochem. Soc. 142 (2) (1995) 326–332.
[29] H. Li, X. Huang, L. Chen, Z. Wu, Y. Liang, A high capacity nano Si composite anode material for lithium rechargeable batteries, Electrochem. Solid-State Lett. 2 (11) (1999) 547–549.
[30] R. Teki, M.K. Datta, R. Krishnan, T.C. Parker, T.M. Lu, P.N. Kumta, N. Koratkar, Nanostructured silicon anodes for lithium ion rechargeable batteries, Small 5 (20) (2009) 2236–2242.
[31] K. Peng, X. Wang, L. Li, Y. Hu, S. Lee, Silicon nanowires for advanced energy conversion and storage, Nano Today 8 (1) (2013) 75–97.
[32] X.H. Liu, L.Q. Zhang, L. Zhong, Y. Liu, H. Zheng, J.W. Wang, J.H. Cho, S.A. Dayeh, S.T. Picraux, J.P. Sullivan, Ultrafast electrochemical lithiation of individual Si nanowire anodes, Nano Lett. 11 (6) (2011) 2251–2258.
[33] Y. Zhou, X. Jiang, L. Chen, J. Yue, H. Xu, J. Yang, Y. Qian, Novel mesoporous silicon nanorod as an anode material for lithium ion batteries, Electrochim. Acta 127 (2014) 252–258.
[34] F.H. Du, K.X. Wang, J.S. Chen, Strategies to succeed in improving the lithium-ion storage properties of silicon nanomaterials, J. Mater. Chem. A 4 (1) (2016) 32–50.
[35] H. Wu, G. Chan, J.W. Choi, I. Ryu, Y. Yao, M.T. McDowell, S.W. Lee, A. Jackson, Y. Yang, L. Hu, Y. Cui, Stable cycling of double-walled silicon nanotube battery anodes through solid-electrolyte interphase control, Nat. Nanotechnol. 7 (5) (2012) 310–315.
[36] H. Wu, Y. Cui, Designing nanostructured Si anodes for high energy lithium ion batteries, Nano Today 7 (5) (2012) 414–429.
[37] S.H. Nguyen, J.C. Lim, J.K. Lee, Electrochemical characteristics of bundle-type silicon nanorods as an anode material for lithium ion batteries, Electrochim. Acta 74 (2012) 53–58.
[38] Y. Yao, M.T. McDowell, I. Ryu, H. Wu, N. Liu, L. Hu, W.D. Nix, Y. Cui, Interconnected silicon hollow nanospheres for lithium-ion battery anodes with long cycle life, Nano Lett. 11 (7) (2011) 2949–2954.
[39] Z. Qian, A. Akisanya, An investigation of the stress singularity near the free edge of scarf joints, Eur. J. Mech.-A/Solids 18 (3) (1999) 443–463.
[40] A. Akisanya, N. Fleck, Interfacial cracking from the freeedge of a long bi-material strip, Int. J. Solids Struct. 34 (13) (1997) 1645–1665.
[41] A. Rao, Stress concentrations and singularities at interface corners, ZAMM-J. Appl. Math. Mech. 51 (5) (1971) 395–406.
[42] V. Hein, F. Erdogan, Stress singularities in a two-material wedge, Int. J. Fract. Mech. 7 (3) (1971) 317–330.
[43] S. Suresh, Graded materials for resistance to contact deformation and damage, Science 292 (5526) (2001) 2447–2451.
[44] J. Aboudi, M.J. Pindera, S.M. Arnold, Higher-order theory for functionally graded materials, Compos. Part B 30 (8) (1999) 777–832.
[45] H. Yao, H. Gao, Gibson-soil-like materials achieve flaw-tolerant adhesion, J. Comput. Theor. Nanosci. 7 (7) (2010) 1299–1305.
[46] Z. Guo, L. Zhou, H. Yao, Improving the electrochemical performance of Si-based anode via gradient Si concentration, Mater. Des. 177 (2019) 107851.
[47] Y. Gao, H. Yao, Homogenizing interfacial shear stress via thickness gradient, J. Mech. Phys. Solids 131 (2019) 112–124.
[48] Q. Yin, Z. Guo, Y. Li, H. Yao, Computational study on the effects of mechanical constraint on the performance of Si nanosheets as anode materials for lithium-ion batteries, J. Phys. Chem. C 122 (28) (2018) 16374–16379.
[49] M. Barber, T.S. Sun, E. Petrach, X. Wang, Q. Zou, Contact mechanics approach to determine contact surface area between bipolar plates and current collector in proton exchange membrane fuel cells, J. Power Sources 185 (2) (2008) 1252–1256.